

MHD mixed convection flow in a vertical lid-driven square enclosure including a heat conducting horizontal circular cylinder with Joule heating

M.M. Rahman, M.A. Alim

Department of Mathematics
Bangladesh University of Engineering and Technology
Dhaka-1000, Bangladesh
m71ra@yahoo.com

Received: 2009-08-15 **Revised:** 2010-03-09 **Published online:** 2010-06-01

Abstract. In the present numerical investigation we studied the effect of magnetohydrodynamic (MHD) mixed convection flow in a vertical lid-driven square enclosure including a heat conducting horizontal circular cylinder with Joule heating. The governing equations along with appropriate boundary conditions for the present problem are first transformed into a non-dimensional form and the resulting non linear system of partial differential equations are then solved numerically using Galerkin's finite element method. Parametric studies of the fluid flow and heat transfer in the enclosure are performed for magnetic parameter (Hartmann number) Ha , Joule heating parameter J , Reynolds number Re and Richardson number Ri . The streamlines, isotherms, average Nusselt number at the hot wall and average temperature of the fluid in the enclosure are presented for the parameters. The numerical results indicated that the Hartmann number, Reynolds number and Richardson number have strong influence on the streamlines and isotherms. On the other hand, Joule heating parameter has little effect on the streamline and isotherm plots. Finally, the mentioned parameters have significant effect on average Nusselt number at the hot wall and average temperature of the fluid in the enclosure.

Keywords: magnetohydrodynamic, Joule heating, finite element method, mixed convection, lid driven enclosure.

Nomenclature

| | | | |
|-------|--|-------|--|
| B_0 | magnetic induction [Wb/m ²] | J | Joule heating parameter |
| c_p | specific heat at constant pressure | k | thermal conductivity of fluid [Wm ⁻¹ K ⁻¹] |
| D | dimensionless diameter of the cylinder | k_s | thermal conductivity of cylinder [Wm ⁻¹ K ⁻¹] |
| g | gravitational acceleration [ms ⁻²] | K | solid fluid thermal conductivity ratio |
| Gr | Grashof number | L | length of the enclosure [m] |
| h | convective heat transfer coefficient [Wm ⁻² K ⁻¹] | Nu | Nusselt number |
| Ha | Hartmann number | | |

| | | | |
|------------|---|-----------|--|
| p | dimensional pressure [Nm^{-2}] | u, v | dimensional velocity components [ms^{-1}] |
| P | dimensionless pressure | U, V | dimensional velocity components |
| Re | Reynolds number | U_0 | lid velocity [m/s] |
| Ri | Richardson number | \bar{V} | enclosure volume [m^3] |
| T | dimensional temperature [K] | x, y | Cartesian coordinates [m] |
| ΔT | dimensional temperature difference [K] | X, Y | dimensionless Cartesian coordinates |

Greek symbols

| | |
|----------|--|
| α | thermal diffusivity [m^2s^{-1}] |
| β | thermal expansion coefficient [K^{-1}] |
| ν | kinematic viscosity [m^2s^{-1}] |
| θ | non dimensional temperature |
| ρ | density of the fluid [kg m^{-3}] |
| μ | dynamic viscosity of the fluid [m^2s^{-1}] |
| σ | fluid electrical conductivity [$\Omega^{-1}\text{m}^{-1}$] |

Subscripts

| | |
|------|---------|
| av | average |
| c | cold |
| h | heated |
| s | solid |

1 Introduction

Combined free and forced convective flow in lid-driven cavities occurs as a result of two competing mechanisms. The first is due to shear flow caused by the movement of one of the walls in the enclosure, while the second is due to buoyancy flow produced by thermal non-homogeneity of the enclosure boundaries. Analysis of mixed convective flow in a lid-driven enclosure finds applications in materials processing, flow and heat transfer in solar ponds, dynamics of lakes, reservoirs and cooling ponds, crystal growing, float glass production, metal casting, food processing, galvanizing, and metal coating, among others. There have been many investigations in the past on mixed convective flow in lid-driven cavities. Many different configurations and combinations of thermal boundary conditions have been considered and analyzed by various investigators.

Moallemi and Jang [1] studied numerically mixed convective flow in a bottom heated square lid-driven enclosure. They investigated the effect of Prandtl number on the flow and heat transfer process. They found that the effects of buoyancy are more pronounced for higher values of Prandtl number, and they also derived a correlation for the average Nusselt number in terms of the Prandtl number, Reynolds number and Richardson number. Iwatsu et al. [2] made numerical simulations for the flow of a viscous thermally stratified fluid in a square cavity. The flow was driven by both the top lid and buoyancy. Later on, Iwatsu et al. [3] and Iwatsu and Hyun [4] conducted respectively two- and three-dimensional numerical simulation of mixed convection in a square cavity heated from the top moving wall. Prasad and Koseff [5] reported experimental results for mixed convection in deep lid-driven cavities heated from below. They observed that the heat transfer was rather insensitive to the Richardson number. Aydin and Yang [6] numerically studied mixed convection heat transfer in a two-dimensional square cavity having an aspect ratio of 1. Steady state two-dimensional mixed convection problem in a

vertical two-sided lid-driven differentially heated square cavity investigated numerically by Oztop and Dagtekin [7]. At the same time, Gau and Sharif [8] numerically studied mixed convection heat transfer in a two-dimensional rectangular cavity with constant heat flux from partially heated bottom wall while the isothermal sidewalls are moving in the vertical direction. Braga and Lemos [9] numerically studied steady laminar natural convection within a square cavity filled with a fixed amount of conducting solid material consisting of either circular or square obstacles.

Rudraiah et al. [10] studied the effect of a magnetic field on free convection in a rectangular enclosure. The problem of unsteady laminar combined forced and free convection flow and heat transfer of an electrically conducting and heat generating or absorbing fluid in a vertical lid-driven cavity in the presence of a magnetic field was formulated by Chamkha [11]. Mahmud et al. [12] studied analytically a combined free and forced convection flow of an electrically conducting and heat-generating/absorbing fluid in a vertical channel made of two parallel plates under the action of transverse magnetic field.

In the present paper the main objective is to examine the flow and heat transfer in a lid-driven square enclosure with the presence of a magnetic field, Joule heating and heat conducting horizontal circular cylinder. The same physical configuration, except the solid cylinder and Joule heating term was investigated numerically by Chamkha [11].

2 Physical model

The physical model considered here is shown in Fig. 1(a), along with the important geometric parameters.

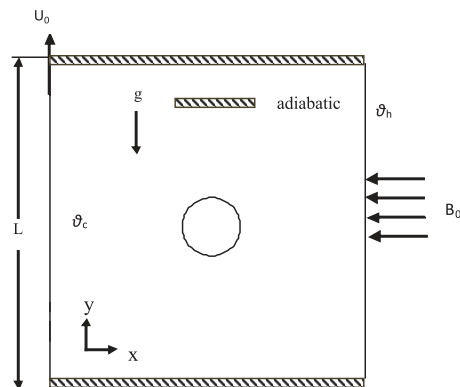


Fig. 1(a). Schematic diagram of the physical model.

A Cartesian co-ordinate system is used with the origin at the lower left corner of the computational domain. It consists of a vertical lid-driven square enclosure with sides of length L , filled with an electrically conducting fluid and a heat conducting horizontal

circular solid cylinder of diameter $D = 0.2$. A uniform magnetic field is applied in the horizontal direction normal to the vertical walls. Both the top and bottom walls are assumed to be adiabatic while the left and the right walls are maintained at constant and different temperatures θ_c and θ_h respectively such that $\theta_h > \theta_c$. The left wall of the enclosure is allowed to move in its own plane at a constant velocity U_0 . The working fluid is assigned a Prandtl number of 0.71 throughout this investigation. All physical properties of fluid are assumed to be constant except density variation in the body force term of the momentum equation according to the Boussinesq approximation.

3 Mathematical formulation

Under the usual Boussinesq assumption, the governing equations for the present problem can be described in dimensionless form by the following equations

$$\frac{\partial U}{\partial X} + \frac{\partial V}{\partial Y} = 0, \quad (1)$$

$$U \frac{\partial U}{\partial X} + V \frac{\partial U}{\partial Y} = -\frac{\partial P}{\partial X} + \frac{1}{Re} \left(\frac{\partial^2 U}{\partial X^2} + \frac{\partial^2 U}{\partial Y^2} \right), \quad (2)$$

$$U \frac{\partial V}{\partial X} + V \frac{\partial V}{\partial Y} = -\frac{\partial P}{\partial Y} + \frac{1}{Re} \left(\frac{\partial^2 V}{\partial X^2} + \frac{\partial^2 V}{\partial Y^2} \right) + Ri \theta - \frac{Ha^2}{Re} V, \quad (3)$$

$$U \frac{\partial \theta}{\partial X} + V \frac{\partial \theta}{\partial Y} = \frac{1}{Re Pr} \left(\frac{\partial^2 \theta}{\partial X^2} + \frac{\partial^2 \theta}{\partial Y^2} \right) + JV^2. \quad (4)$$

For solid

$$\frac{\partial^2 \theta_s}{\partial X^2} + \frac{\partial^2 \theta_s}{\partial Y^2} = 0. \quad (5)$$

The dimensionless variables are defined as:

$$X = \frac{x}{L}, \quad Y = \frac{y}{L}, \quad U = \frac{u}{U_0}, \quad V = \frac{v}{U_0},$$

$$P = \frac{p}{\rho U_0^2}, \quad \theta = \frac{T - T_c}{T_h - T_c}, \quad \theta_s = \frac{T_s - T_c}{T_h - T_c}.$$

The governing parameters in the preceding equations are the Reynolds number Re , Grashof number Gr , Hartmann number Ha , Joule heating parameter J , Prandtl number Pr , Richardson number Ri , and solid fluid thermal conductivity ratio K which are defined in the following:

$$Re = \frac{U_0 L}{\nu}, \quad Gr = \frac{g \beta \Delta T L^3}{\nu^2}, \quad Ha^2 = \frac{\sigma B_0^2 L^2}{\mu}, \quad J = \frac{\sigma B_0^2 L U_0}{\rho C_p \Delta T},$$

$$Pr = \frac{\nu}{\alpha}, \quad Ri = \frac{Gr}{Re^2} \quad \text{and} \quad K = \frac{k_s}{k_f}.$$

The associated dimensionless boundary conditions are

$$\begin{aligned}
U = 0, \quad V = 1, \quad \theta = 0 & \quad \text{at the left wall,} \\
U = 0, \quad V = 0, \quad \theta = 1 & \quad \text{at the right vertical wall,} \\
U = 0, \quad V = 0 & \quad \text{at the cylinder surface,} \\
U = 0, \quad V = 0, \quad \frac{\partial \theta}{\partial N} = 0 & \quad \text{at the top and bottom walls,} \\
\left(\frac{\partial \theta}{\partial N} \right)_{fluid} = K \left(\frac{\partial \theta_s}{\partial N} \right)_{solid} & \quad \text{at the fluid-solid interface.}
\end{aligned}$$

The average Nusselt number at the heated wall of the enclosure is defined as $Nu = - \int_0^1 \frac{\partial \theta}{\partial X} dY$ and the bulk average temperature in the enclosure is defined as $\theta_{av} = \int \frac{\theta}{V} dV$, where N is the non-dimensional distances either along X or Y direction acting normal to the surface and V is the enclosure volume.

4 Method of solution

The methodology proposed for analyzing mixed convection in an obstructed vented cavity in our previous paper Rahman et al. [13] is employed here to investigate the mixed convection in an obstructed lid-driven cavity with slight modification. In this method, the continuum domain is divided into a set of non-overlapping regions called elements. Six node triangular elements with quadratic interpolation functions for velocity as well as temperature and linear interpolation functions for pressure are utilized to discretize the physical domain. Moreover, interpolation functions in terms of local normalized element coordinates are employed to approximate the dependent variables within each element. Substitution of the obtained approximations into the system of the governing equations and boundary conditions yields a residual for each of the conservation equations. These residuals are reduced to zero in a weighted sense over each element volume using the Galerkin method.

The velocity and thermal energy equations result in a set of non-linear coupled equations for which an iterative scheme is adopted. The application of this technique and the discretization procedures are well documented by Taylor and Hood [14] and Dechaumphai [15]. The convergence of solutions is assumed when the relative error for each variable between consecutive iterations is recorded below the convergence criterion ε such that

$$\sum |\phi_{ij}^m - \phi_{ij}^{m-1}| \leq \varepsilon,$$

where ϕ represents a dependent variable U, V, P , and θ , the indexes i, j indicate a grid point, and the index m is the current iteration at the grid level. The convergence criterion was set to 10^{-5} .

5 Grid refinement test

In order to obtain grid independent solution, a grid refinement test were performed for an obstructed lid-driven square enclosure at respective values of $Re = 100$, $Ri = 1.0$, $Ha = 10.0$, and $J = 1.0$. Using a triangular mesh for two-dimensional simulation, five different meshes were used of which, 38229 nodes and 5968 elements provided satisfactory spatial resolution for the base case geometry as shown in the Table 1 and the solution was found to be independent of the grid size with further refinement. The mesh mode for the present numerical computation is shown in Fig. 1(b).

Table 1. Grid sensitivity test at $Re = 100$, $Ri = 1.0$, $Ha = 10.0$, and $J = 1.0$.

| Nodes (elements) | 24427 (3774) | 29867 (4640) | 37192 (5814) | 38229 (5968) | 48073 (7524) |
|---------------------|-----------------|-----------------|-----------------|-----------------|-----------------|
| Nu | 1.022636 | 1.022643 | 1.022650 | 1.022651 | 1.022651 |
| θ_{av} | 0.509055 | 0.509056 | 0.509055 | 0.509056 | 0.509056 |
| Time [s] | 380.953 | 490.594 | 651.422 | 708.953 | 1046.390 |

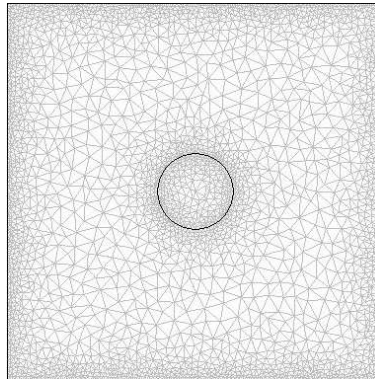


Fig. 1(b). Continuum domain of the schematic diagram.

6 Code validation

The present numerical code is verified against a documented numerical study. Namely, the numerical solution reported by Chamkha [11], which is based on a finite volume scheme. The findings of the comparisons are documented in Table 2 and Table 3 for the average Nusselt number. The comparisons illustrate close proximity in the predictions made between the various solutions. These validation cases boost up the confidence in the numerical outcome of the present work.

Table 2. Effect of Ha on Nu for $Gr = 100$, $Pr = 0.71$, $Re = 1000$, and $\Delta = 0$.

| Parameter Ha | Present study Nu | Chamkha [11] Nu | Error (%) |
|-------------------|-----------------------|----------------------|-----------|
| 0.0 | 2.206915 | 2.2692 | 2.75 |
| 10.0 | 2.113196 | 2.1050 | 0.82 |
| 20.0 | 1.820612 | 1.6472 | 10.53 |
| 50.0 | 1.18616 | 0.9164 | 29.44 |

Table 3. Effect of Gr on Nu for $Ha = 0$, $Pr = 0.71$, $Re = 100$, and $\Delta = 0$.

| Parameter Gr | Present study Nu | Chamkha [11] Nu | Error (%) |
|-------------------|-----------------------|----------------------|-----------|
| 10^2 | 1.029805 | 0.9819 | 4.88 |
| 10^3 | 1.105932 | 1.0554 | 4.78 |
| 10^4 | 1.523059 | 1.4604 | 4.29 |
| 10^5 | 2.462188 | 2.3620 | 4.24 |

7 Results and discussion

The implications of varying the Hartmann number (Ha), Joule heating parameter (J) Reynolds number (Re), and Richardson number (Ri), in the enclosure will be emphasized. The results are presented in terms of streamlines and isotherm patterns. The variations of average Nusselt number and average temperature are also highlighted. The solid fluid thermal conductivity ratio $K = 5.0$ have considered throughout the simulation. Physically, this value of K represents a solid body of wood in a gas with properties similar to those of air.

Fig. 2 depicts the influence of Hartmann number Ha on the flow and temperature fields where $Re = 100$, $Ri = 1.0$, and $J = 1.0$ are kept fixed. In Fig. 2(a)(i), it can be observed that in the absence of the magnetic field ($Ha = 0$), there developed two unequal vortices of opposite directions. The vortex with clockwise (CW) direction has developed along the left surface, which is expected, since the lid is driven from the bottom to top. In the right part of the enclosure the flow is counterclockwise (CCW) because of the presence of buoyancy force. Now looking into Figs. 2(a)(ii)–(iii) that are for $Ha = 10.0$ and 20.0 , it can be explained that the flow rate of the vortices near the left surface increases in size. We may further observe that for $Ha = 50.0$ the CW vortex near the left wall occupy the maximum part of the enclosure where as the CCW vortex near the heated surface become reduces in size and turn into two small eddies as shown in Fig. 2(a)(iv). It means that the magnetic field strongly affects the flow field. The effects of Hartmann number Ha on the isotherms are shown in the Figs. 2(b)(i)–(iv). From these figures it can be seen easily that the isotherms are almost parallel to the right vertical wall for the higher values of Ha ($Ha = 50.0$), indicating that most of the heat transfer process is carried out by conduction. Some deviations of isothermal lines are observed near the top surface in the enclosure at the lower values of Ha due to the buoyancy induced large CCW vortex.

In order to evaluate how the presence of the magnetic fields affects the heat transfer rate along the hot wall, average Nusselt number is plotted as a function of Richardson number (Ri) as shown in Fig. 3. It is observed that average Nusselt number increases with increase of Ri and it is always higher for the small values of Ha ($Ha = 0.0$). Another examination of Fig. 3 does reveal that up to a Ri of 1.0, average fluid temperature (θ_{av}) in the enclosure is lower for the small values of Ha , but after this it lower for the large values of Ha .

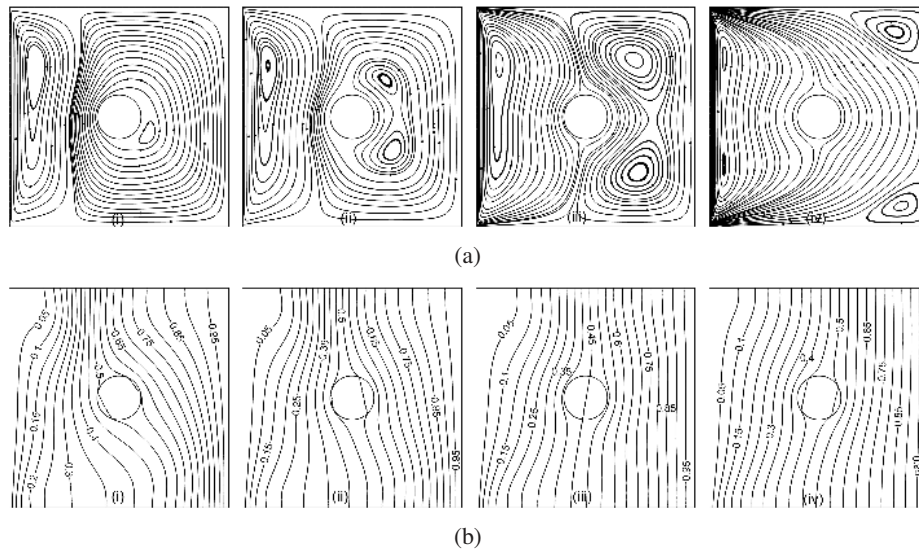


Fig. 2. (a) streamlines and (b) isotherms for (i) $Ha = 0.0$, (ii) $Ha = 10.0$, (iii) $Ha = 20.0$, and (iv) $Ha = 50.0$ while $Re = 100$, $Ri = 1.0$, and $J = 1.0$.

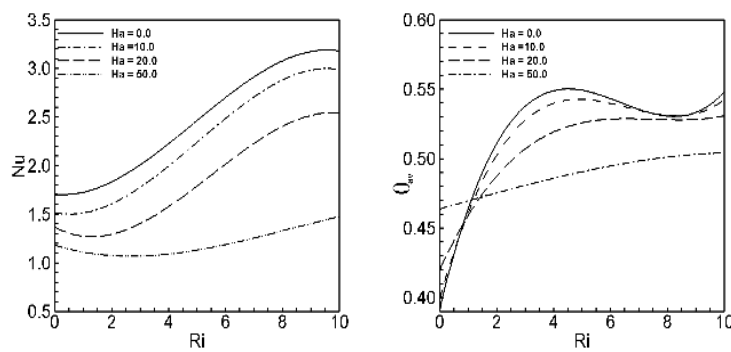


Fig. 3. Effect of Ha on average Nusselt number and average temperature while $Re = 100$, $K = 5.0$, $J = 0.0$, and $D = 0.2$.

Figs. 4(a)(i)–(iv) and 4b(i–iv) show the distribution of the streamlines and isotherms for $J = 0.0, 0.5, 1.0$ and 2.0 at $Re = 100$, $Ri = 1.0$, and $Ha = 10.0$ respectively. At $J = 0.0$, the circulation of the flow in the enclosure shows two overall counter rotating asymmetric eddies as shown in Fig. 4(a)(i). For $J = 0.5, 1.0$, and 2.0 the pattern of the streamlines are almost identical that is for $J = 0.0$. However, a careful observation indicates that the core of the counterclockwise (CCW) eddy remains unchanged for $J = 0.0, 0.5$, and 1.0 , but it becomes large for $J = 2.0$. On the other hand, the size of the clockwise (CW) eddy remains unchanged for different values of J . Now from the Fig. 4(b)(i)–(iv), it can be seen that a plume starts to appear on the top side in the enclosure at $J = 0.0$. The plume near the right top corner gradually increases and near the left top corner gradually decreases with increasing values of J . Only a thin thermal boundary is seen near the left wall of the enclosure for the large value of $J = 2.0$.

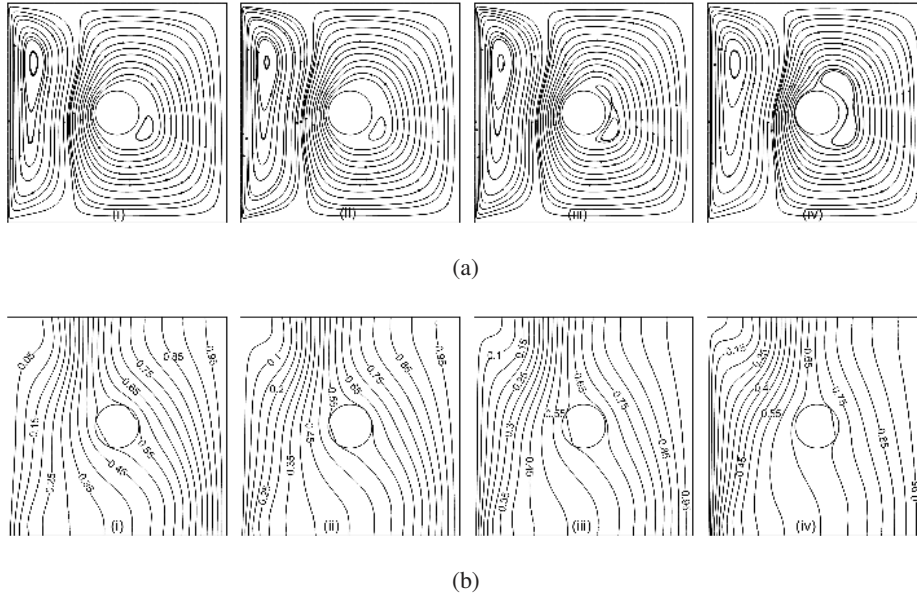


Fig. 4. (a) streamlines and (b) isotherms for (i) $J = 0.0$, (ii) $J = 0.5$, (iii) $J = 1.0$, and (iv) $J = 2.0$ while $Re = 100$, $Ha = 10.0$, and $Ri = 1.0$.

The average Nusselt number (Nu) at the hot wall of the enclosure as a function of Richardson number (Ri) for the four different Joule heating parameters is shown in Fig. 5. It is observed that for $J = 0.0$, Nu increases, but for $J = 0.5$, and 1.0 , Nu shows oscillatory behavior and for $J = 2.0$, Nu decreases with the increase of Ri . It is also note that Nu is always higher for $J = 0.0$. Fig. 5 also explains the average temperature of the fluid in the enclosure as a function of Richardson number (Ri) for the four different J . With increasing Ri the average temperature increases and the lower value of θ_{av} is observed for $J = 0.0$.

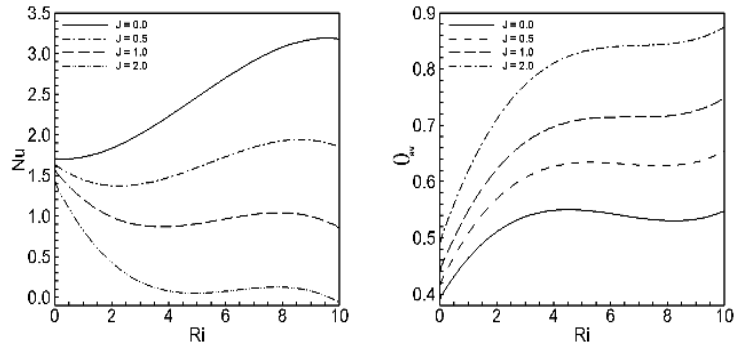


Fig. 5. Effect of J on average Nusselt number and average temperature while $Re = 100$, $D = 0.2$, $K = 5.0$ and $Ha = 10.0$.

Fig. 6 illustrates the impact of Re on the variation of the streamlines and isotherms for $Ri = 1.0$, $Ha = 10.0$, and $J = 1.0$. For a relatively small Reynolds number, i.e., $Re = 50$, there exists 3 recirculation cells as shown in the Fig. 6(a)(i). Among the cells, a clockwise (CW) cell occupying maximum part of the enclosure and the other two small counterclockwise (CCW) cells developed near the right top and bottom corner in the enclosure. This implies that fluid is well mixed in the enclosure. With the increasing values of Re , ($Re = 100, 150, 200$) the size of the CCW cell adjacent to the right vertical

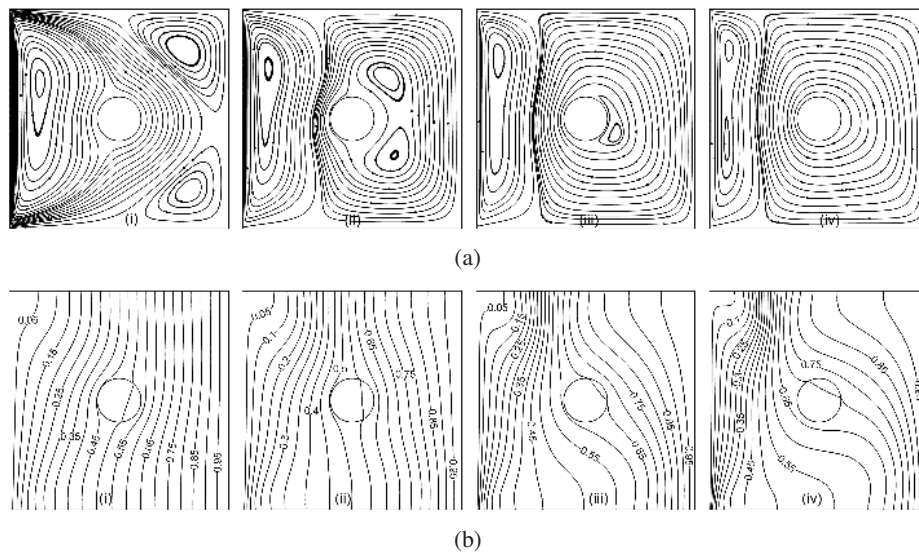


Fig. 6. (a) streamlines and (b) isotherms for (i) $Re = 50$, (ii) $Re = 100$, (iii) $Re = 150$, and (iv) $Re = 200$ while $Ri = 1.0$, $Ha = 10.0$, and $J = 1.0$.

heated wall gradually increases and occupies almost the enclosure, pushing down the CW cell near the left vertical wall and this is because of the increase of shear force. Corresponding temperature distributions can be seen in Figs. 6(b)(i)–(iv). From these figures it can be seen that, isothermal lines are nearly parallel to the hot wall for $Re = 50$, which is similar to conduction-like distribution. Isothermal lines at $Re = 100$ start to turn back from the cold wall due to the dominating influence of the convective current. At $Re = 150$ and 200, convective distortion of the isotherms occurs throughout the enclosure due to the strong influence of the convective current.

The effect of the Reynolds number on the average Nusselt number at the heat source and the average temperature in the enclosure are displayed as a function of Richardson number for some particular Reynolds number as in Fig. 7. It is observed that the average Nusselt number for different Reynolds number shows an oscillatory phenomenon with increasing Ri . It is also noting that Nu is always upper for bigger values of Re . On the other hand, the average temperature is lesser for $Re = 100$ up to $Ri \leq 0.5$, and after this it is lesser for $Re = 200$.

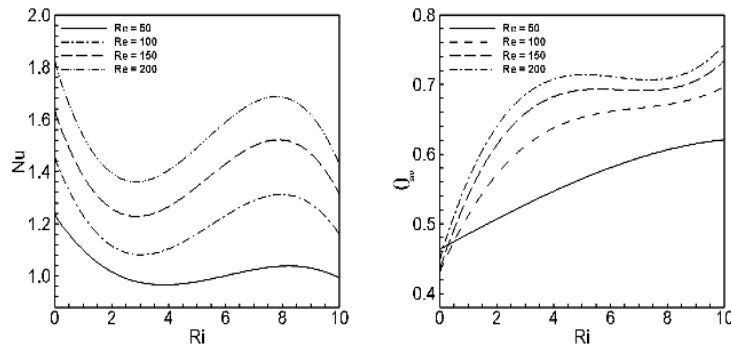


Fig. 7. Effect of Reynolds number on average Nusselt number and average temperature while $D = 0.2$, $K = 5.0$, $Ha = 10.0$, and $J = 1.0$.

The sensitivity of the streamlines and isotherms patterns due to the variation in Richardson number is presented in Fig. 8(i)–(iv) for $Re = 100$, $Ha = 10.0$, and $J = 1.0$. It can be seen in the Fig. 8(a)(i) that for pure forced convection ($Ri = 0.0$) there exists only one clockwise (CW) recirculation cell, whose core is an egg shape located near the left top corner of the enclosure. From the Fig. 8(a)(ii) it can be seen easily that for $Ri = 2.5$, the CW cell becomes small in size dramatically and a large counterclockwise (CCW) cell is developed near the heated wall. On the other hand, the core of the CW cell becomes into two small eddies. Further increasing values of the Richardson number ($Ri = 5.0, 10.0$) increases the strength of the CCW cell as well as decreases the CW cell. These effects of Richardson number on the flow field are reasonable since increasing values of Ri assists buoyancy forces. If we examine carefully the Fig. 8(a)(iv), it can be seen that the core of the CCW cell take an egg shaped pattern around the cylinder. The significant influence of Ri on isotherm patterns are presented in Fig. 8(b)(i)–(iv). From

the Fig. 8(b)(i) it can be seen that the isothermal lines near the heated surface become parabolic for $Ri = 0.0$, whereas for a further change of Ri to 2.5 the isothermal lines also become parabolic near the cold surface as shown in Fig. 8(b)(ii). The corresponding effect of the increasing buoyancy force ($Ri = 5.0, 10.0$) on the isotherms are shown in Fig. 8(b)(iii)–(iv). From these figures it can ascertain that increase in the buoyancy force causes the isotherms to deform increasingly and a thermal boundary layer form near the cold surface.

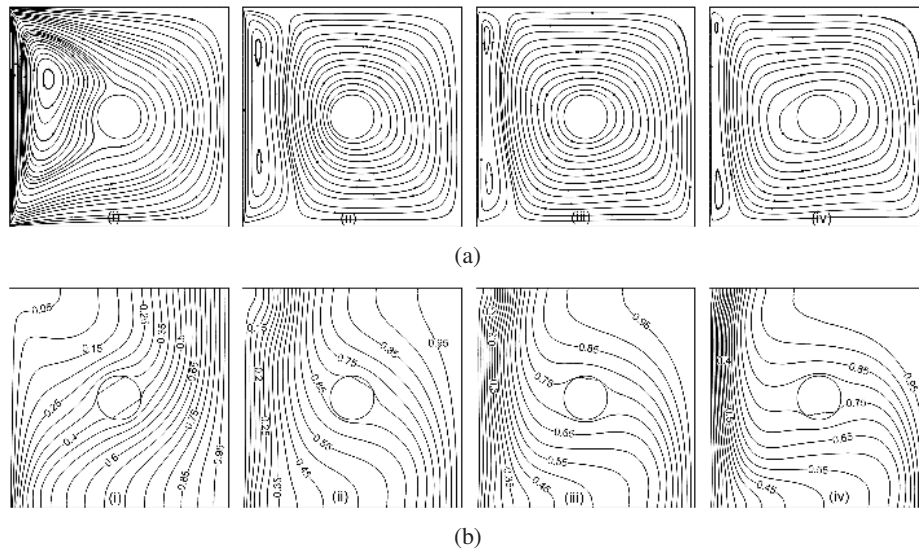


Fig. 8. (a) streamlines and (b) isotherms for (i) $Ri = 0.0$, (ii) $Ri = 2.5$, (iii) $Ri = 5.0$, and (iv) $Ri = 10.0$, while $Re = 100$, $K = 5.0$, $D = 0.2$, $Ha = 10.0$, and $J = 1.0$.

8 Conclusion

The following major conclusions may be drawn from the present investigations:

- The heat transfer and the flow characteristics inside the enclosure depend strongly upon the strength of the magnetic field.
- A little effect of the Joule heating parameters on the streamlines and isotherms is observed. The overall heat transfer decreases with the increase of J and the lowest average temperature in the enclosure is found for $J = 0.0$.
- Reynolds number Re affects strongly the streamlines and isotherm structures in the enclosure. Higher heat transfer rates is observed for large Re . Average temperature in the enclosure become lesser for $Re = 100$ at $Ri \leq 0.5$, and after this it is lesser for $Re = 50$.

- Mixed convection parameter Ri affects significantly on the flow structure and heat transfer inside the enclosure.

References

1. M.K. Moallemi, K.S. Jang, Prandtl number effects on laminar mixed convection heat transfer in a lid-driven cavity, *Int. J. Heat Mass Tran.*, **35**, pp. 1881–1892, 1992.
2. R. Iwatsu, J.M. Hyun, K. Kuwahara, Numerical simulation of flows driven by a torsionally oscillating lid in a square cavity, *J. Fluids Eng.*, **114**, pp. 143–151, 1992.
3. R. Iwatsu, J.M. Hyun, K. Kuwahara, Mixed convection in a driven cavity with a stable vertical temperature gradient, *Int. J. Heat Mass Tran.*, **36**, pp. 1601–1608, 1993.
4. R. Iwatsu, J.M. Hyun, Three-dimensional driven cavity flows with a vertical temperature gradient, *Int. J. Heat Mass Tran.*, **38**, pp. 3319–3328, 1995.
5. A.K. Prasad, J.R. Koseff, Combined forced and natural convection heat transfer in a deep lid-driven cavity flow, *Int. J. Heat Fluid Fl.*, **17**, pp. 460–467, 1996.
6. O. Aydin, W.J. Yang, Mixed convection in cavities with a locally heated lower wall and moving side walls, *Numer. Heat Tr: A-Appl.*, **37**, pp. 695–710, 2000.
7. H.F. Oztop, I. Dagtekin, Mixed convection in two-sided lid-driven differentially heated square cavity, *Int. J. Heat Mass Tran.*, **47**, pp. 1761–1769, 2004.
8. G. Guo, M.A.R. Sharif, Mixed convection in rectangular cavities at various aspect ratios with moving isothermal side walls and constant flux heat source on the bottom wall, *Int. J. Therm. Sci.*, **43**, pp. 465–475, 2004.
9. E.J. Braga, M.J.S. de Lemos, Laminar natural convection in cavities filled with circular and square rods, *Int. Commun. Heat Mass*, **32**, pp. 1289–1297, 2005.
10. N. Rudraiah, R.M. Barron, M. Venkatachalappa, C.K. Subbaraya, Effect of magnetic field on free convection in a rectangular enclosure, *Int. J. Eng. Sci.*, **33**, pp. 1075–1084, 1995.
11. A.J. Chamkha, Hydromagnetic combined convection flow in a vertical lid-driven cavity with internal heat generation or absorption, *Numer. Heat Tr: A-Appl.*, **41**, pp. 529–546, 2002.
12. S. Mahmud, S.H. Tasnim, M.A.H. Mamun, Thermodynamic analysis of mixed convection in a channel with transverse hydromagnetic effect, *Int. J. Thermal Sciences*, **42**, pp. 731–740, 2003.
13. M.M. Rahman, M.A. Alim, M.A.H. Mamun, Finite element analysis of mixed convection in a rectangular cavity with a heat-conducting horizontal circular cylinder, *Nonlinear Anal. Model. Control*, **14**(2), pp. 217–247, 2009.
14. C. Taylor, P. Hood, A numerical solution of the Navier–Stokes equations using finite element technique, *Comput. Fluids*, **1**, pp. 73–89, 1973.
15. P. Dechaumphai, *Finite Element Method in Engineering*, 2nd ed., Chulalongkorn University Press, Bangkok, 1999.